JOURNAL OF SOLID STATE CHEMISTRY **138,** 7–17 (1998)
ARTICLE NO. SC977692

Synthesis and Properties of $Sr_{1-x}La_xMo_5O_8$ ($0 \leq x \leq 1$): A New Class of Oxides with Metallic Properties

W. H. McCarroll,* M. Borgia,* K. V. Ramanujachary,†,[1] M. Greenblatt,† Patrick Gougeon,‡ and John E. Greedan§

*Chemistry Department, Rider University, Lawrenceville, New Jersey 08648-3099; †Department of Chemistry, Rutgers The State University of New Jersey, Piscataway, New Jersey 08855-0939; ‡Université de Rennes 1, Laboratoire de Chimie du Solide et Inorganique Moléculaire, URA CNRS No 1495, Av. du Général Leclerc, 35042 Rennes Cedex, France; and §Brockhouse Institute for Materials Research, McMaster University 1280 Main St. West, Hamilton, Ontario, Canada L8S 4M1

Received July 10, 1997; in revised form November 3, 1997; accepted November 4, 1997

Single crystal and oriented polycrystal specimens of the solid solution between $SrMo_5O_8$ and $LaMo_5O_8$ have been prepared by fused salt electrolysis. The La/Sr ratios of the solid solution members formed are highly sensitive to the melt composition. Both end members of this series are semiconducting at room temperature, with the La compound displaying complex low-temperature behavior. On the other hand the solid solutions become metallic over the range 300–20 K when a few atom % of either La or Sr are present. Detailed structural investigations by single crystal X-ray and powder neutron diffraction at ambient and low temperatures failed to reveal any changes in the Mo–Mo or Mo–O network that would account for the observed anomalies in the electronic properties. The composition-controlled semiconductor-to-metal transition can be explained on the basis of a simple qualitative band model. © 1998 Academic Press

INTRODUCTION

A considerable amount of data now exists on the crystallographic and electronic properties of low-valent molybdenum oxides containing strong metal bonds either in the form of clusters or as extended metal–metal bonded chains. The stability of these units appears to be strongly dependent on the number of electrons available for metal–metal bonding in the cluster, the so-called metal cluster electron count (MCE). In general, variable MCEs are not observed in strictly isomorphous systems and when they do occur, significant distortions of the metal–metal bonded units can be expected. Thus, the ability to vary the average valence of molybdenum monotonically without significant changes in the cluster structure has been severely limited.

As an example of this problem we will consider those very interesting systems which contain infinite chains of bonded Mo atoms formed by trans-edge sharing Mo_6 octahedra. For instance, in $NaMo_4O_6$, a member of the most symmetrical subclass of this type of system (1), tetragonally distorted Mo_6 octahedra share *trans*-edges to form infinite linear chains having the composition Mo_4O_6. KMo_4O_6 and $InMo_4O_6$, which have the same MCE (13 electrons), are isomorphous (2, 3). However, in $Ba_{0.62}Mo_4O_6$, which is orthorhombic, these chains are more distorted, ostensibly because of the MCE change. In addition, the unit cell is at least a factor five larger (4, 5). Although the basic building block remains the same, the structures of the subclasses typified by $Ho_4Mo_4O_{11}$, $Zn_{1.25}Sc_{0.75}Mo_4O_7$, $Mn_{1.5}Mo_8O_{11}$, and $ZnMo_8O_{10}$, in which the MCEs range from 14 to 15, display dramatic differences (6–8).

In contrast, the class of compounds having the composition AMo_5O_8 (A = Ca, Sr, Ba, Pb, Sn, Eu, La, Ce, Pr, Nd, Sm, and Gd) is notable in that these compounds apparently can tolerate a change in MCE induced by the valence of the A cation without a significant change in the basic structure of the compound. The structural type AMo_5O_8 has been previously described in detail by several authors (9–14). Its basic structural building block is the double-cluster unit $Mo_{10}O_{18}$, which results from the metal–edge condensation of two Mo_6O_{12}-type clusters (Fig. 1). One therefore can visualize these units as the dimer in a series of oligomers in which $NaMo_4O_6$ represents an example of a phase with the infinite polymer chain. However in AMo_5O_8-type phases, the $Mo_{10}O_{18}$ cluster units are linked on opposite edges via common O atoms to form infinite chains in which the Mo_{10} clusters are strongly bonded through intercluster Mo–Mo bonds [Mo1–Mo1, Mo1–Mo2 ($\times 2$), and Mo1–Mo3 ($\times 2$)] (see Figs. 1 and 2). The shortest interconnecting distance is about 2.68–2.69 Å when A is trivalent, but increases to 2.77–2.80 Å when it is divalent. These chains, which run

[1]Present Address: Rowan University, Department of Chemistry and Physics, Glassboro, New Jersey 08028-1701.

0022-4596/98 $25.00

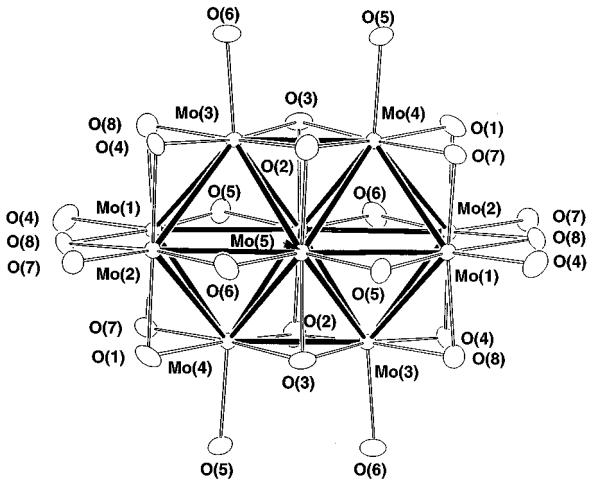

FIG. 1. Bi-Octahedral Mo_{10} cluster (shown as an $Mo_{10}O_{26}$ unit) found in AMo_5O_8 compounds.

parallel to the *a*-axis, are then interlinked through O atoms to create one-dimensional channels where the cations reside. Recent studies of the electronic properties of several of these compounds using single crystal specimens have shown that all are semiconductors (15, 16).

In the cases where A = La, Ce, Nd, Pr, or Sm, an anomalous semiconductor-to-metal transition is observed near 180 K, followed by a re-entrant behavior to the semiconducting state between 30 and 50 K. However, for $SrMo_5O_8$, semiconducting behavior is observed at all temperatures, along with a significant increase in resistivity, i.e., 20 and 400 times higher depending on the temperature. Magnetic susceptibility measurements of all of these compounds show no anomalies which correspond to those seen in the resistivity data (15, 16).

Since earlier studies (15) had demonstrated that it was possible to grow single crystal specimens of both $LaMo_5O_8$ and $SrMo_5O_8$ by fused salt electrolysis, we decided to grow single crystals of their solid solutions and see what effects, if any, fine tuning of the MCE in this system would have on the electrical and magnetic properties. No temperature-dependent structural studies have been reported for any of these materials, so the role of crystallographic phase transitions or more subtle changes in bond distance or angles in determining the resistivity anomalies was unknown. To address this point we have carried out temperature-dependent structural studies of $LaMo_5O_8$ by high resolution neutron diffraction experiments and examined the structure of selected members of the solid solution by single crystal X-ray diffraction methods.

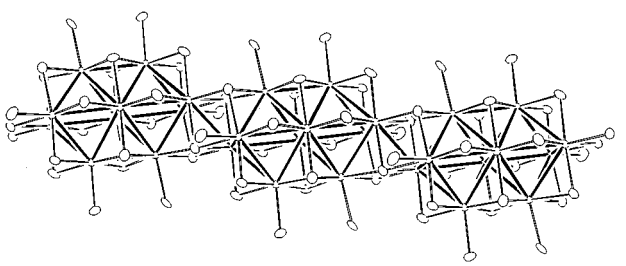

FIG. 2. Infinite chains formed by corner sharing Mo_{10} clusters. Only the shortest intercluster bond (Mo(1)–Mo(1)) is shown.

EXPERIMENTAL

Synthesis and Chemical Analysis

The crystals used in this study were grown by the electrolysis of melts obtained from mixtures of anhydrous sodium molybdate, molybdenum (VI) oxide, lanthanum oxide, and strontium molybdate. The lanthanum oxide and strontium molybdate were ignited at 600 and 800°C for 8 h and stored in a desiccator, while sodium molybdate in the form of dihydrate was rendered anhydrous by drying for 48 h at 160°C. Reagent grade strontium carbonate was sometimes used to optimize the composition of an existing melt, which allowed us to modify the relative amounts of MoO_3 and $SrMoO_4$ in a single step. The electrolyses were carried out in air at 975–1000°C using MacDanel 998 high density alumina crucibles having a volume of 25 cc. A typical charge weighed between 30 and 40 g. A slotted MacDanel cylinder was sometimes used to separate the cathode and anode regions, but was dispensed with when it was observed that it had no marked effect on the quality or quantity of product obtained. A spiral wound from 0.38 mm diameter Pt wire served as the cathode, while the anode was a 1–2 cm^2 Pt plate. Runs were terminated by removing the electrodes from the melt and air quenching the product. The highly crystalline, black product adheres to the cathode and is freed of matrix by alternate washes in hot 5% K_2CO_3–2% ethylenediaminetetraaceticacid solution and 2F HCl.

Attack of the crucible is always a problem and inevitably results in the codeposition of corundum crystals when electrolyses are carried out for long time periods. This is not considered serious when selecting individual samples for resistivity or magnetic measurements. Chemical analysis for metal constituents was carried out using a Baird Atomic inductively coupled plasma emission spectrometer (ICP) with solutions prepared from 20–30 mg of finely ground samples that were decomposed in about 5 cc of hot 6F HNO_3. Solution is completed by the addition of a few drops of 3F HCl before dilution in a volumetric flask. The results are considered to be accurate to between 1 and 2%; i.e., typical of the ICP method. The purity of the products was initially verified by powder X-ray diffraction methods using a Rigaku D-Max 2 system and graphite monochromatized copper radiation. Accurate lattice constants were obtained using a least squares program employing 15 to 20 selected

reflections in the $2\theta = 30°$–$90°$ region. Silicon was used as an internal standard.

The polycrystalline sample of $LaMo_5O_8$ used for the neutron diffraction studies was prepared by a classical solid state reaction. Starting reagents were La_2O_3 (Rhône-Poulenc, 99.999%), MoO_3 (Strem Chemicals, 99.9%) and Mo, all in powder form. The rare earth sesquioxide was prefired at 1000°C before use and the Mo powder was heated under a hydrogen flow at 1000°C for 6 h. The stoichiometric mixture was pressed into pellets and loaded into a molybdenum crucible which was sealed under a low argon pressure using an arc welding system. Pure powder samples could be obtained by heating the charge at the rate of 300°C/h to 1600°C and holding for 48 h. The charge was then cooled at 100°C/hr to 1100°C, and finally furnace cooled.

Diffraction Studies

Two single crystals from the samples 111-23 and 10D1-79 (see Table 1) were selected for X-ray structure determinations. The intensity data were collected on a CAD4 Enraf-Nonius diffractometer using graphite-monochromatized Mo$K\alpha$ radiation ($\lambda = 0.71073$ Å) at room temperature. The lattice constants were determined by least-squares refinement of the setting angles of 25 reflections in the 2Θ range 13°–47°, which had been automatically centered on the diffractometer. For each crystal, three standard reflections were measured every 90 min; they showed no significant variation in intensity during data collections. The intensity data sets were corrected for Lorentz and polarization effects, and empirical absorptions were applied based on azimuthal scans of nine reflections (17). Both structures were refined in the space group $P2_1/c$. Positional parameters of $SrMo_5O_8$ (10) were used in the first stages of the refinements. The final refinement cycles included the atomic coordinates, anisotropic displacement parameters (ADP) for all atoms, and site occupancy factors for the Sr/La sites. The sum of the site occupancy factors was constrained to the unity, as confirmed by ICP analyses, and the ADPs of the La and Sr atoms were constrained to be equal. Calculations were performed on a Digital Pentium Celebris 590 FP for SHELXL-93 (18) and on a Digital microVAX 3100 for the MOLEN (19, 20) programs (data reduction and absorption corrections.)

Powder neutron diffraction data were collected at the DUAL SPEC diffractometer at the Atomic Energy of Canada Ltd. facility in Chalk River, Canada. Neutrons of wavelength 1.3297(2) Å were used. The sample was held in a vanadium can sealed with an indium gasket under helium exchange gas and cooled in a liquid helium cryostat. Temperature control was ± 0.1 K.

TABLE 1
Analyzed Compositions and Unit Cell Data for $Sr_{1-x}La_xMo_5O_8$ Phases

Sample ID	Composition	a (Å)	b (Å)	c (Å)	β (°)	Vol. (Å^3)
3L37	$SrMo_5O_8$	7.559(1)	9.157(1)	9.967(1)	109.29(1)	651.2(2)
10-9	$Sr_{0.955}La_{0.026}Mo_5O_8$	7.561(1)	9.154(1)	9.957(2)	109.28(1)	650.5(1)
10D1-79	$Sr_{0.835}La_{0.163}Mo_5O_8$	7.570(1)	9.142(1)	9.952(2)	109.27(2)	650.1(2)
84-74	$Sr_{0.555}La_{0.433}Mo_5O_8$	7.585(1)	9.114(1)	9.945(2)	109.22(1)	649.2(1)
5B-45	$Sr_{0.533}La_{0.477}Mo_5O_8$	7.587(2)	9.111(3)	9.932(4)	109.21(3)	648.3(5)
8MA-73	$Sr_{0.520}La_{0.480}Mo_5O_8$	7.588(1)	9.106(1)	9.936(2)	109.22(1)	648.3(1)
8L-72	$Sr_{0.296}La_{0.700}Mo_5O_8$	7.583(1)	9.100(2)	9.921(3)	109.11(1)	646.9(3)
8K-72	$Sr_{0.299}La_{0.714}Mo_5O_8$	7.588(1)	9.097(2)	9.924(2)	109.14(2)	647.2(2)
111-23	$Sr_{0.113}La_{0.892}Mo_5O_8$	7.578(1)	9.094(1)	9.919(1)	109.10(1)	645.9(1)
111-24	$Sr_{0.070}La_{0.918}Mo_5O_8$	7.576(1)	9.091(1)	9.916(1)	109.07(1)	645.5(1)
80-15A	$Sr_{0.010}La_{1.003}Mo_5O_8$	7.574(1)	9.089(1)	9.915(1)	109.03(1)	645.2(1)
XI-174	$Sr_{0.005}La_{1.007}Mo_5O_8$	7.574(1)	9.089(1)	9.916(1)	109.04(1)	645.3(1)
X-47-5C	$La_{1.005}Mo_5O_8$	7.571(1)	9.088(1)	9.917(1)	109.04(1)	645.0(1)

Resistivity and Magnetic Measurements

Electrical resistivity measurements were carried out in a four-point probe configuration using a closed cycle refrigeration system (APD cryogenics, Model DE 202) over the temperature range 20–300 K. The I-V profiles were monitored at regular temperature intervals to verify the ohmic nature of the ultrasonically soldered indium contacts. The current was passed parallel to the crystallographic a-axis (i.e., parallel to the plate) based on the crystal habit of the sample as correlated with previous oscillation and Weissenberg X-ray photography studies. Measurements of magnetic susceptibilities were carried out on batches of randomly oriented crystals with a Quantum Design SQUID magnetometer (MPMS) at temperatures 5–300 K. The applied field was 0.5 Tesla.

RESULTS AND DISCUSSION

Crystal Synthesis and Composition

The composition of the product obtained is highly sensitive to the composition of the melt. To prepare pure $SrMo_5O_8$, we used a melt which had approximate molar ratios of $Na_2MoO_4 : MoO_3 : SrMoO_4 = 18.0 : 1.0 : 4.5$, while for pure $LaMo_5O_8$ the corresponding ratios were $Na_2MoO_4 : MoO_3 : La_2O_3 = 2.5 : 1.0 : 0.41$. In the case of $LaMo_5O_8$ synthesis, small departures from these values produced various reduced phases such as $La_2Mo_2O_7$, $La_5Mo_4O_{16}$, $La_9Mo_{15}Al_2O_{42}$, and $LaMo_2O_5$ when La was in slight excess. However when MoO_3 was in excess, $LaMo_{7.7}O_{14}$, $La_{1+x}Mo_8O_{16}$, MoO_2, and a phase with a composition similar to $La_5Mo_{32}O_{54}$ were the cathode products. Thus, it was necessary to make small additions to the melt of MoO_3, La_2O_3, $SrCO_3$, or $SrMoO_4$ until a narrow region of melt composition was found for which single phase $Sr_{1-x}La_xMo_5O_8$ could be deposited. To prepare the solid solutions rich in Sr, we added small amounts of La_2O_3

to the melt previously used to prepare $SrMo_5O_8$. Indeed, only small additions of La were necessary to produce substantial incorporation of this species. For instance, when the formal Sr : La ratio in the melt was 50 : 1, the resultant product contained 19 atomic % of La on the *A* site, while approximately 50 atomic % of La was incorporated at a formal Sr : La ratio of 14 : 1. On the other hand, substantial amounts of $SrMoO_4$ had to be added to the La-rich melt to introduce noticeable amounts of Sr into La-rich crystals; e.g., a mole ratio of La : Sr = 1.6 : 1.0, as determined by ICP analysis of a melt sample, yielded a solid solution containing only 0.5 atomic % Sr. Similarly, only about 7.0 atomic % Sr incorporation was achieved when the analyzed ratio of La : Sr in the melt was about 100 : 1. Although $SrMoO_4$ is quite soluble in Na_2MoO_4 at the temperatures used, the presence of MoO_3 at the levels used for the synthesis of pure $LaMo_5O_8$ resulted in the formation of a precipitate when $SrMoO_4$ was present in significant quantities. Hence the relative amounts of MoO_3 in the melts had to be drastically reduced for successful synthesis of Sr-rich phases, although even then some small amount of an unknown precipitate remained. Nonetheless, the addition of MoO_3 to the melt was absolutely necessary to establish a melt composition in which $SrMo_5O_8$; or Sr-rich solid solutions could be obtained.

Table 1 gives a summary of the results of the chemical analysis for metal content along with unit cell data obtained for several samples. The chemical formulas are derived from the observed molar ratios of the metals and are based on the assumption of full stoichiometry for molybdenum and oxygen based on the general formula AMo_5O_8. The presence of corundum as a possible contaminant had been established by prior X-ray diffraction and microscopic analysis. The amounts of this impurity observed correlated well with the length of time the crucible had been in use. No sample was chosen for analysis whose X-ray diffraction pattern showed any evidence of corundum. In spite of these efforts to select corundum-free samples for analysis, small amounts of an insoluble, transparent, crystalline residue were observed by microscopic examination of some of the analytical solutions. Thus any analysis for oxygen "by difference" would be meaningless. The total of La and Sr are, within analytical error, indicative of full stoichiometry for the *A* position, which is consistent with all prior single crystal structure studies of these phases. However, small variations in stoichiometry cannot be ruled out.

The precise crystal habit and size and perfection of the crystals obtained seem to depend on the relative amounts of La and Sr present. Pure $LaMo_5O_8$ has a well-defined, oblique, tabular or plate-like crystal habit, typically with bright reflecting surfaces. The unique axis of the monoclinic cell corresponds to the face normal of the plate. Heavy intergrowth of these plates occurs, but fragments up to 1 mm in size can be found free of apparent intergrowths.

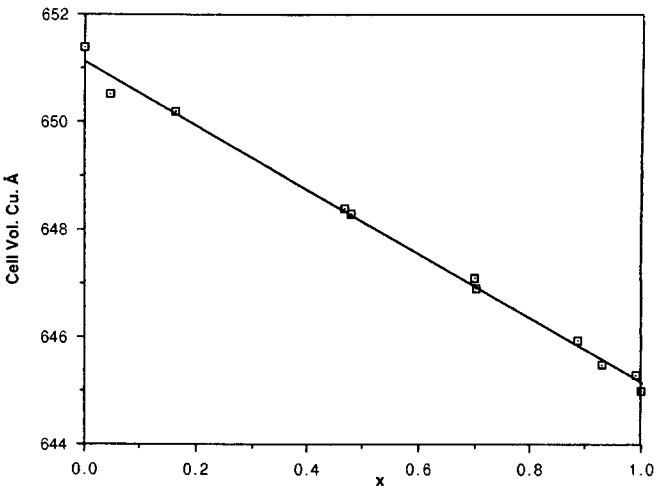

FIG. 3. Vegards law plot for the $Sr_{1-x}La_xMo_5O_8$ solid solution series.

Samples lightly doped with Sr (e.g., sample 111-23) are very similar in crystal habit to the pure lanthanum compound. On the other hand, pure $SrMo_5O_8$ and other samples rich in Sr tend to form as large plate-like agglomerates with ill-defined edges or as dendritic growths which have a feather-like aspect. The plate-like agglomerates usually have bright plate faces and typically are 1–3 mm in largest dimension with thicknesses of 0.3–0.6 mm. It was these specimens that were chosen for electrical and magnetic measurements of the pure Sr and Sr-rich solid solutions.

Table 1 also summarizes the lattice constants based on space group $P2_1/c$ and unit cell volumes for each of the chemically analyzed samples. Fig. 3 shows an essentially linear compositional dependence on the unit cell volume which allowed us to use these values as rough estimates of the Sr/La ratios in the solid solutions for routine work.

Crystal Structure

A single crystal structural study was carried out on two members of the solid solution system in an attempt to ascertain whether any structural changes were observed that might be correlated with changes in the electrical or magnetic properties. Unfortunately all specimens taken from samples with approximately equi-molar amounts of Sr and La were found to be twinned.

The details of the X-ray single crystal data collections and structure refinements for $Sr_{0.90}La_{0.10}Mo_5O_8$ and $Sr_{0.11}La_{0.89}Mo_5O_8$ are summarized in Table 2. Final positional and equivalent isotropic displacement parameters are listed in Tables 3 and 4. Selected interatomic distances are given in Table 5 and compared to those observed in $SrMo_5O_8$ (10) and $LaMo_5O_8$ (11).

Examination of Table 5 reveals that the various interatomic distances in $Sr_{0.90}La_{0.10}Mo_5O_8$ and $Sr_{0.11}La_{0.89}$

TABLE 2
Crystallographic and Experimental Data for $Sr_{0.898(5)}La_{0.102(5)}Mo_5O_8$ and $Sr_{0.11(6)}La_{0.889(5)}Mo_5O_8$

Formula	$Sr_{0.898(5)}La_{0.102(5)}Mo_5O_8$	$Sr_{0.111(6)}La_{0889(5)}Mo_5O_8$
Molecular weight	700.55	740.92
Crystal system	Monoclinic	
Space group	$P21/c$	
a (Å)	7.569(3)	7.571(2)
b (Å)	9.147(2)	9.090(2)
c (Å)	9.957(3)	9.910(2)
β (°)	109.28(1)	109.107(8)
V (Å)	650.7(4)	644.5(2)
Density (calc., g.cm^{-3})	7.151	7.636
Temperature (K)	293	
Diffractometer	Enraf-Nonius CAD4	
Radiation	Mo$K\alpha$ radiation ($\lambda = 0.71073$Å)	
Crystal color	Black	
Morphology	Irregular	
Crystal size (mm^3)	$0.10 \times 0.09 \times 0.07$	$0.10 \times 0.09 \times 0.08$
Linear absorption coeff. (mm^{-1})	17.32	16.12
Monochromator	Oriented graphite	
Scan mode	ω–2θ	
Recording range 2θ (°)	2–90	
hkl range	0/15, 0/18, −19/18	
No. of measured reflections	5595	5543
No. of independent reflections	5338	5289
Rint	0.0186	0.0324
Absorption correction	Ψ scan	
Transmission (min–max)	0.204–0.298	0.239–0.275
Refinement	F^2	
Calculated weight		
$w = 1/[\sigma^2(Fo^2) + (aP)^2 + bP]$	$a = 0.0251$	$a = 0.0132$
where $P = (Fo^2 + 2Fc^2)/3$	$b = 5.3508$	$b = 8.4478$
Extinction coefficient	0.0058(2)	0.0102(2)
$R[F^2 > 2(F^2)]$	0.0344	0.0273
$R(F^2)$ on all data	0.0537	0.0329
w$R(F^2)$ on all data	0.0810	0.0672
S (all data)	1.274	1.328
No. of refined parameters	130	130
Largest ΔF peaks (e/Å^3)	2.786/−2.699	2.753/−2.876

TABLE 3
Fractional Atomic Coordinates and Equivalent Isotropic Displacement Parameters for $Sr_{0.898(5)}La_{0.102(5)}Mo_5O_8$

Atom	x	y	z	U_{eq}[a]
La	0.25489(5)	0.50421(4)	0.53850(3)	0.00702(9)
Sr	0.25489(5)	0.50421(4)	0.53850(3)	0.00702(9)
Mo1	0.61001(4)	−0.11428(3)	0.48325(3)	0.00269(5)
Mo2	0.38056(4)	−0.11630(3)	0.68111(3)	0.00296(5)
Mo3	0.17816(4)	−0.12617(3)	0.38688(3)	0.00274(5)
Mo4	0.81234(4)	−0.13204(3)	0.29909(3)	0.00277(5)
Mo5	−0.00136(4)	−0.12213(3)	0.58614(3)	0.00264(4)
O1	0.3947(4)	0.0057(3)	0.8406(3)	0.0060(4)
O2	0.0049(4)	−0.2240(3)	0.9353(3)	0.0045(3)
O3	−0.0084(3)	0.0004(3)	0.2362(3)	0.0048(3)
O4	0.4014(3)	−0.2549(3)	0.0198(3)	0.0042(3)
O5	0.7990(4)	−0.2484(3)	0.1178(3)	0.0049(4)
O6	0.2020(4)	−0.2468(3)	0.2161(3)	0.0052(4)
O7	0.6042(4)	−0.2393(3)	0.8272(3)	0.0055(4)
O8	0.3861(3)	−0.0017(3)	0.3323(3)	0.0047(3)

Note. $\tau(Sr) = 0.898(5)$; $\tau(La) = 0.102(5)$.
[a] $U_{eq} = 1/3\sum_i\sum_j U_{ij}a_i^*a_j^*a_ia_j$.

Mo_5O_8 differ only slightly from those observed in the two respective end members of the solid solution $SrMo_5O_8$ and $LaMo_5O_8$. In fact, previous X-ray structure studies have shown that the Mo–Mo bond distances most affected by the charge and to a smaller extent by the size of the cation are those between the Mo_{10} clusters [Mo1–Mo1, Mo1–Mo2, and Mo1–Mo3]. We have thus represented in Fig. 4 the variation of these three intercluster distances as function of the ionic radii of the cations. The latter ones were taken as the difference between the average A–O distances and the ionic radius of O^{2-}. The increasing size of the cation, which is well exemplified by the trivalent rare-earth compounds (Gd–La), only leads to small, nearly linear variations of the three different intercluster bonds. When the cationic charge is modified, changes in the intercluster Mo–Mo distances are observed which are not commensurate with the average ionic radius of the A site cations. This behavior is particularly sensitive in the two La–Sr compounds with $x = 0.11$ and 0.90, both of which only differ by about 0.2 e^- per Mo_{10} from $SrMo_5O_8$ and $LaMo_5O_8$. Concerning the intracluster distances, the largest variation in length is about 0.04 Å as one moves from $SrMo_5O_8$ to $LaMo_5O_8$. However, the general trend is a slight increase of the average of the Mo–Mo distances within the Mo_{10} cluster from 2.740 Å when A is divalent to 2.749 Å when it is trivalent. For $Sr_{0.90}La_{0.10}Mo_5O_8$ and $Sr_{0.11}La_{0.89}Mo_5O_8$, the mean

TABLE 4
Fractional Atomic Coordinates and Equivalent Isotropic Displacement Parameters for $Sr_{0.111(6)}La_{0.889(5)}Mo_5O_8$

Atom	x	y	z	U_{eq}[a]
La	0.26080(3)	0.50422(2)	0.53961(2)	0.00558(5)
Sr	0.26080(3)	0.50422(2)	0.53961(2)	0.00558(5)
Mo1	0.60553(3)	−0.11478(3)	0.48577(3)	0.00327(4)
Mo2	0.38274(3)	−0.11745(3)	0.67746(3)	0.00347(4)
Mo3	0.17408(3)	−0.12685(3)	0.38362(3)	0.00285(4)
Mo4	0.80889(3)	−0.12998(3)	0.29792(3)	0.00276(4)
Mo5	−0.00247(3)	−0.12225(3)	0.58622(3)	0.00289(4)
O1	0.3966(3)	0.0057(3)	0.8477(2)	0.0053(3)
O2	−0.0002(3)	−0.2224(3)	0.9338(3)	0.0049(3)
O3	−0.0122(3)	0.0023(3)	0.2315(2)	0.0046(3)
O4	0.3935(3)	−0.2493(3)	0.0136(3)	0.0057(3)
O5	0.7955(3)	−0.2434(3)	0.1149(2)	0.0048(3)
O6	0.2003(3)	−0.2414(3)	0.2099(3)	0.0058(3)
O7	0.6048(3)	−0.2363(3)	0.8285(3)	0.0053(3)
O8	0.3842(3)	−0.0056(3)	0.3284(2)	0.0051(3)

Note. $\tau(Sr) = 0.111(6)$; $\tau(La) = 0.889(5)$.
[a] $U_{eq} = 1/3\sum_i\sum_j U_{ij}a_i^*a_j^*a_ia_j$.

TABLE 5
Selected Bond Distances (Å)

	$SrMo_5O_8$	$Sr_{0.89}La_{0.10}Mo_5O_8$	$Sr_{0.11}La_{0.89}Mo_5O_8$	$LaMo_5O_8$
Mo(1)–Mo(2)	2.6905(6)	2.6848(6)	2.6787(5)	2.6816(5)
Mo(1)–Mo(4)	2.7507(6)	2.7546(8)	2.7806(5)	2.7876(5)
Mo(1)–Mo(5)	2.7672(6)	2.7768(7)	2.8053(7)	2.8094(5)
Mo(1)–Mo(3)	2.7740(7)	2.7781(13)	2.8054(6)	2.8124(5)
Mo(1)–Mo(1)[a]	2.7651(9)	2.7608(8)	2.6986(6)	2.6890(7)
Mo(1)–Mo(2)[a]	3.0380(6)	3.0261(9)	2.9244(6)	2.9108(5)
Mo(1)–Mo(3)[a]	3.0869(6)	3.0897(14)	3.0890(7)	3.0911(5)
Mo(2)–Mo(5)	2.7196(6)	2.7292(13)	2.7304(6)	2.7609(5)
Mo(2)–Mo(4)	2.7413(7)	2.7424(7)	2.7565(7)	2.7288(5)
Mo(2)–Mo(3)	2.8263(6)	2.8237(9)	2.8233(6)	2.8279(5)
Mo(3)–Mo(4)	2.6034(6)	2.6145(12)	2.6133(6)	2.6102(5)
Mo(3)–Mo(5)	2.6950(6)	2.6941(7)	2.6757(6)	2.6727(5)
Mo(3)–Mo(5)	2.7494(6)	2.7502(8)	2.7525(5)	2.7558(5)
Mo(4)–Mo(5)	2.7389(6)	2.7393(9)	2.7452(6)	2.7505(5)
Mo(4)–Mo(5)	2.7715(7)	2.7709(7)	2.7608(6)	2.7605(5)
Mo(5)–Mo(5)	2.8324(9)	2.8209(7)	2.8113(7)	2.8172(7)
Mo(1)–O(5)	2.034(4)	2.038(3)	2.040(2)	2.043(3)
Mo(1)–O(7)	2.036(4)	2.040(3)	2.063(2)	2.069(3)
Mo(1)–O(4)	2.104(4)	2.106(3)	2.114(2)	2.113(3)
Mo(1)–O(8)	2.106(4)	2.113(3)	2.122(2)	2.119(3)
Mo(1)–O(8)	2.117(4)	2.124(3)	2.124(2)	2.122(3)
Mo(2)–O(1)	1.902(4)	1.915(3)	1.999(2)	2.009(3)
Mo(2)–O(6)	1.953(4)	1.956(3)	1.987(2)	1.990(3)
Mo(2)–O(4)	2.040(4)	2.039(3)	2.049(2)	2.046(3)
Mo(2)–O(8)	2.117(4)	2.111(3)	2.106(2)	2.110(3)
Mo(2)–O(7)	2.145(4)	2.150(3)	2.142(2)	2.142(3)
Mo(3)–O(3)	2.042(4)	2.046(3)	2.061(2)	2.058(3)
Mo(3)–O(2)	2.058(4)	2.061(3)	2.072(2)	2.072(3)
Mo(3)–O(4)	2.065(4)	2.077(3)	2.070(2)	2.067(3)
Mo(3)–O(6)	2.087(4)	2.084(2)	2.077(2)	2.077(3)
Mo(3)–O(8)	2.148(4)	2.153(3)	2.148(2)	2.146(3)
Mo(4)–O(3)	2.061(4)	2.058(3)	2.073(2)	2.070(3)
Mo(4)–O(7)	2.062(4)	2.065(3)	2.065(2)	2.066(3)
Mo(4)–O(1)	2.070(4)	2.069(3)	2.076(2)	2.078(3)
Mo(4)–O(5)	2.071(4)	2.070(3)	2.060(2)	2.055(3)
Mo(4)–O(2)	2.087(4)	2.096(3)	2.105(2)	2.103(3)
Mo(5)–O(5)	2.023(4)	2.024(3)	2.048(2)	2.055(3)
Mo(5)–O(6)	2.039(4)	2.041(3)	2.040(2)	2.039(3)
Mo(5)–O(2)	2.063(4)	2.070(3)	2.073(2)	2.077(3)
Mo(5)–O(3)	2.065(4)	2.071(3)	2.082(2)	2.086(3)
La–O(1)	2.529(4)	2.525(3)	2.442(2)	2.443(3)
La–O(1)	2.552(4)	2.527(3)	2.465(2)	2.458(3)
La–O(4)	2.597(4)	2.581(3)	2.492(3)	2.487(3)
La–O(7)	2.648(4)	2.635(3)	2.579(3)	2.574(3)
La–O(5)	2.718(4)	2.719(3)	2.677(3)	2.676(3)
La–O(8)	2.750(4)	2.740(3)	2.704(2)	2.704(3)
La–O(3)	2.764(4)	2.755(3)	2.730(2)	2.732(3)
La–O(2)	2.770(4)	2.761(3)	2.753(2)	2.761(3)
La–O(6)	2.930(4)	2.938(3)	2.866(3)	2.860(3)
La–O(2)	2.935(4)	2.946(3)	2.924(2)	2.919(3)

[a] Intercluster distance.

values are 2.742 and 2.747 Å, respectively, in agreement with the progressive increase of the cationic charge and concomitant addition of electrons to the bi-octahedral Mo_{10} cluster.

The Mo–O bond lengths show no well-defined variations with respect to the ionic radius of the cation. On the other hand, the effect of the charge transfer is particularly important on the Mo2–O1 and Mo2–O6 bonds, which increase by about 0.1 and 0.04 Å respectively, when the charge increases by 2 e^- per Mo_{10} cluster ($SrMo_5O_8$ to $LaMo_5O_8$). The overall trend of the Mo–O bonds, is an increase in length with increasing charge of the cations as reflected by the average of the Mo–O bonds, which is 2.062 Å in $SrMo_5O_8$ and 2.076 Å in $LaMo_5O_8$. This is confirmed by $Sr_{0.90}La_{0.10}Mo_5O_8$ and $Sr_{0.11}La_{0.89}Mo_5O_8$ in which the mean values are 2.066 and 2.075 Å, respectively.

Given the remarkable resistivity-vs-temperature behavior of $LaMo_5O_8$ (Fig. 6), it was reasonable to ask whether structural changes play any role. To investigate such a possibility, high-resolution neutron diffraction data were collected for four strategic temperatures, 200, 100, 50, and 5 K. The data shown in Fig. 5 for 100 K are exemplary. There are no discernible differences in the powder patterns at various temperatures. Refinement was accomplished by the Rietveld code, FULLPROF (21). Starting parameters were taken from (11). A total of 60 parameters were refined, including 42 positional parameters and an overall temperature factor. No significant improvement was obtained by including the 14 individual thermal parameters in the refinement.

The results for the 100 K experiment are listed in Tables 6a and 6b. The refined positional parameters agree well with the earlier single crystal study (11). In addition, on inspection of all the results, it was clear that there are no significant changes in any of these parameters as a function of temperature. Table 7 demonstrates a lack of the kind of variation in bond distances and angles which might be expected if structural changes were to be associated with the transport properties of $LaMo_5O_8$ as a function of temperature, i.e., the intercluster distances between Mo(1) and Mo(1), and Mo(2) and Mo(5), and the interchain angles Mo(4)–O(5)–Mo(4) and Mo(3)–O(6)–Mo(3).

Electrical and Magnetic Properties

Figures 6 and 7 show the behavior of the electrical resistivity of the end members of the solid solution as a function of temperature. Both the La and Sr members are semiconductors at room temperature, with the resistivity of the Sr analog being about 20 times higher. In the case of the latter compound, semiconducting behavior is observed throughout the entire range of temperature (300–100 K), the measurements having to be terminated at 100 K because of the high resistance of the sample. On the other hand, $LaMo_5O_8$ displays almost temperature-independent resistivity down to about 180 K, where a broad semiconductor-to-metal transition takes place (15). This transition is followed by a relatively sharp increase in the resistivity at 50 K, indicative of a semiconducting state. This behavior is, in fact, typical of all the trivalent rare earths with this structure, although it is somewhat more complicated in the case of the Gd compound (15). Figures 8 and 9 show the magnetic susceptibilities as a function of temperature for the La and

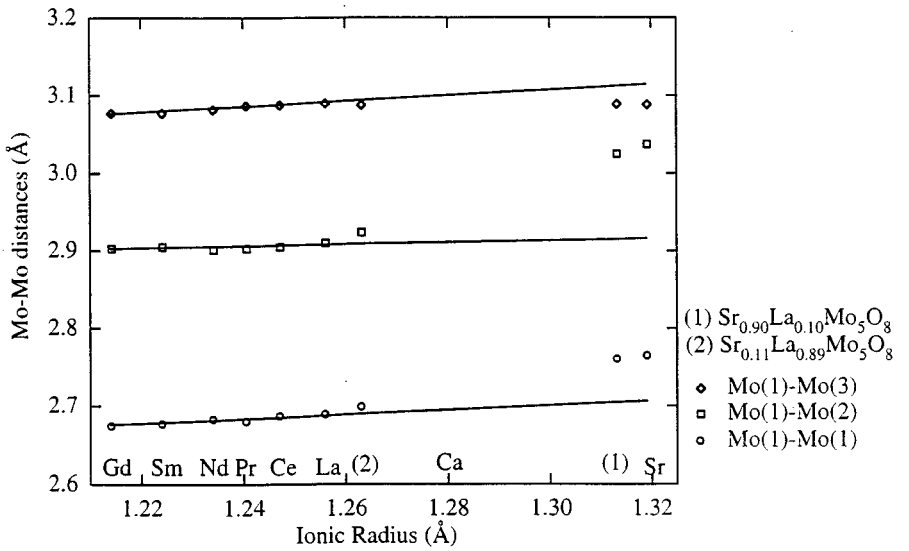

FIG. 4. Variation of intercluster Mo–Mo distances for AMo_5O_8 phases.

Sr compounds. Both show a very weak paramagnetism with the La compound displaying no magnetic anomalies in the regions where such changes were observed in the electrical resistivity.

The formation of a solid solution between these two phases results in remarkable changes in the temperature dependence of their electrical resistivities as compared to the end members. When 0.5–1.5 atom % of Sr is introduced into the La compound, the behavior is very similar to the pure La compound. However, when 7 atom % of Sr is incorporated, the compound displays metallic behavior (Fig. 10). The broad but accelerated decrease in the resistivity around 70 K is not accompanied by concomitant changes in magnetic susceptibility. The origin of this transition is not clear, although this anomaly bears some resemblance to that observed for $LaMo_5O_8$ at $\sim$170 K (see Fig. 6). Samples containing 48 and 16 atom % La, on the other hand, clearly display metallic behavior with a more or less monotonic decrease of resistivity over the entire temperature range (see Figs. 11 and 12). In all cases, the small positive values of the magnetic susceptibilities remained essentially temperature-

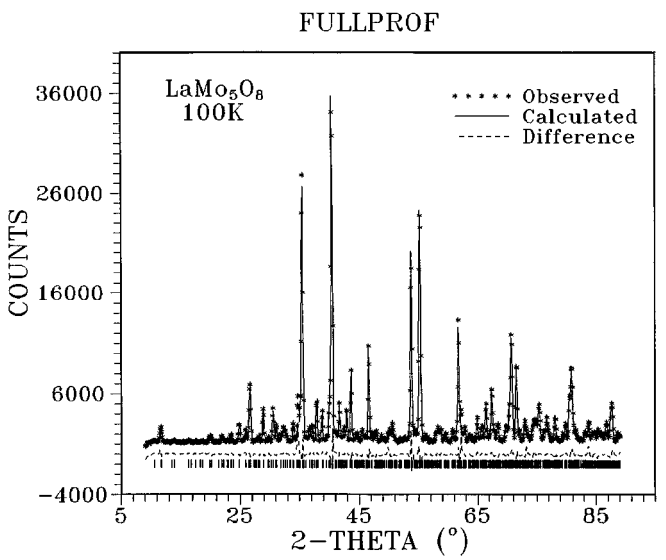

FIG. 5. Rietveld analysis of neutron diffraction data for $LaMo_5O_8$ at 100°K. The asterisks represent the data points, the solid line is the calculated profile, the dashed line is the difference plot, and the vertical tick marks show the Bragg peak positions.

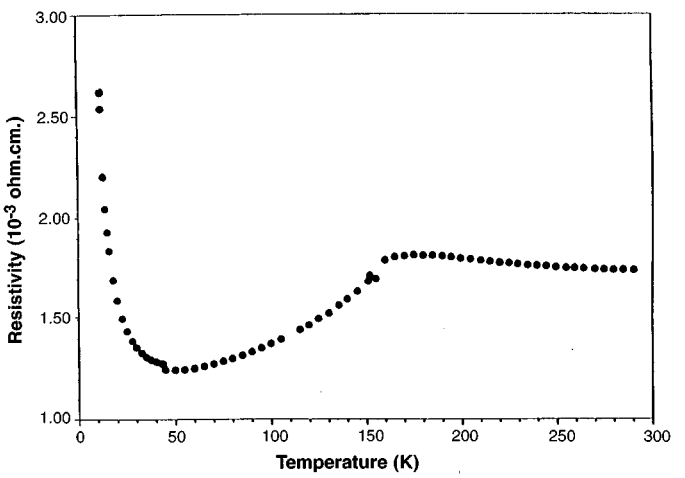

FIG. 6. Temperature variation of the electrical resistivity of $LaMo_5O_8$.

TABLE 6a
Refined Position Parameters for $LaMo_5O_8$ at 100 K in $P2_1/a$

Atom	x	y	z
La	0.0396(11)	0.0023(13)	0.2574(14)
Mo1	0.4879(18)	0.1188(17)	0.6042(21)
Mo2	0.5857(15)	0.1210(17)	0.0039(20)
Mo3	0.3858(15)	0.1280(17)	0.1779(19)
Mo4	0.2990(16)	0.1275(17)	0.8116(20)
Mo5	0.6801(16)	0.1151(15)	0.3880(18)
O1	0.8473(17)	− 0.0061(32)	0.3925(21)
O2	0.9292(22)	0.2218(18)	− 0.0083(29)
O3	0.1180(23)	0.2453(17)	0.7976(27)
O4	0.2055(24)	0.2448(19)	0.1982(29)
O5	0.2313(16)	− 0.0046(21)	− 0.0095(20)
O6	0.0108(31)	0.2497(16)	0.3951(28)
O7	0.8309(25)	0.2284(18)	0.6033(26)
O8	0.3253(18)	0.0020(33)	0.3832(19)

TABLE 7
Intercluster Bond Distances and Interchain Bond Angles in $LaMo_5O_8$ at Various Temperatures

	Intercluster Distances (Å)			
Temperature (K)	200	100	50	5
Mo(1)–Mo(1)	2.76(3)	2.73(3)	2.73(3)	2.74(3)
Mo(1)–Mo(2)	2.91(3)	2.89(3)	2.90(3)	2.90(3)
Mo(1)–Mo(3)	3.07(2)	3.05(2)	3.05(2)	3.05(2)
	Interchain angles (°)			
Mo(4)–O(5)–Mo(4)	167.3(11)	167.7(10)	167.7(10)	167.6(9)
Mo(3)–O(6)–Mo(3)	167.5(11)	168.4(9)	167.7(9)	167.6(9)

independent. A typical plot of the magnetic susceptibility as a function of temperature is shown in Fig. 13 for $Sr_{0.52}La_{0.48}MO_5O_8$. The small cusp seen in the susceptibility near 50 K is attributed to the antiferromagnetic ordering of residual oxygen in the SQUID chamber (22).

Dramatic changes in the electrical resistivities were observed in samples containing small amounts of La added to the semiconducting $SrMo_5O_8$. The electrical resistivity of the sample with approximately 2.6 atom % La in $SrMo_5O_8$ as a function of temperature is shown in Fig. 14. The room-temperature electrical resistivity of the doped sample is nearly an order of magnitude smaller than that observed in the undoped $SrMo_5O_8$ (Fig. 7). In addition, contrasting changes are also seen in the temperature dependence of the resistivity following the addition of a small amount of La. Rather than an exponential increase in resistivity with decreasing temperature as observed in $SrMo_5O_8$, the $Sr_{0.955}La_{0.026}Mo_5O_8$ sample shows nearly temperature-independent behavior down to $\sim$100 K characteristic of a degenerate semiconductor. Furthermore, the sharp upturn observed below 100 K signals a transition to the insulating state with an opening of a gap near the Fermi level. We have considered the possibility that the observed transition to the insulating state is defect-driven (Anderson localization). However, given the sharpness of the transition this appears to be unlikely. Alternatively, in view of the low-dimensional nature of these compounds, as well as changes in the MCEs induced by La doping, the transition could well be due to the onset of a charge density wave. Of course, more detailed studies would be needed to confirm this hypothesis. Because of the difficulties encountered in controlling the precise composition of the crystal and obtaining specimens suitable for resistivity measurements, we are unable to establish the composition where the Sr-rich solid solution becomes metallic. Nevertheless based on the above results, the metal-to-insulator transition clearly appears to occur in the range $x = 0.025$–0.16. On the other hand, metallic behavior in the La-rich region is clearly evident by the time 7 atom % Sr ($x = 0.93$) has been incorporated.

TABLE 6b
Unit Cell Parameters, and Rietveld Agreement Indices for $LaMo_5O_8$ at 200K, 100K, 50K, and 5K

Temperature (K)	200	100	50	5
a (Å)	9.9282(9)	9.9254(9)	9.9243(9)	9.9243(8)
b (Å)	9.0938(7)	9.0952(7)	9.0956(7)	9.0962(7)
c (Å)	7.5734(7)	7.5626(7)	7.5587(7)	7.5580(7)
β (°)	109.038(6)	108.965(6)	108.944(5)	108.933(5)
R_p	0.056	0.055	0.055	0.053
R_{wp}	0.084	0.083	0.083	0.080
R_B	0.065	0.067	0.065	0.065
No. (hkl)	790	790	789	789

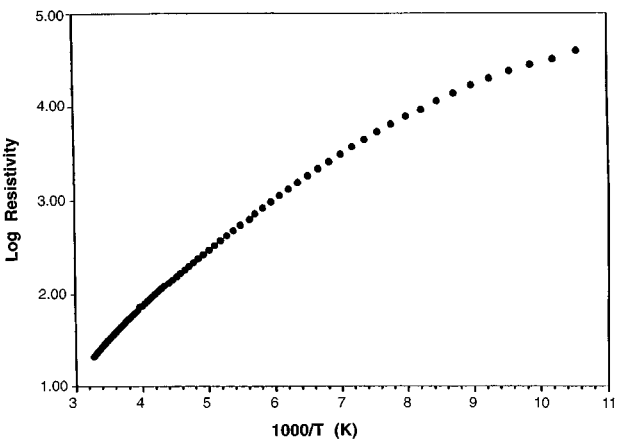

FIG. 7. Temperature variation of the log of electrical resistivity of $SrMo_5O_8$.

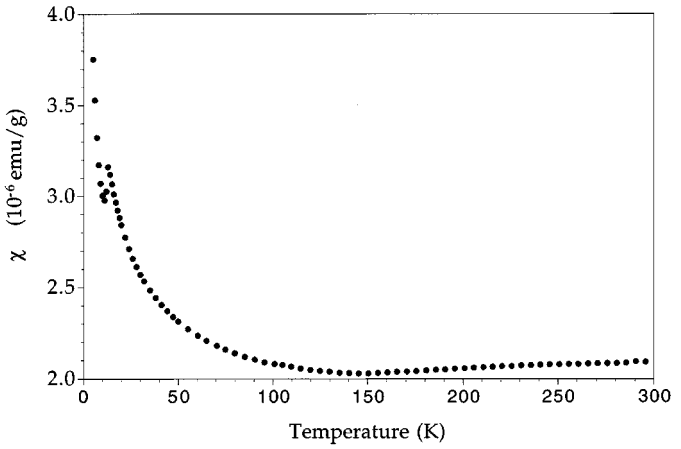

FIG. 8. Temperature variation of the magnetic susceptibility of $LaMo_5O_8$.

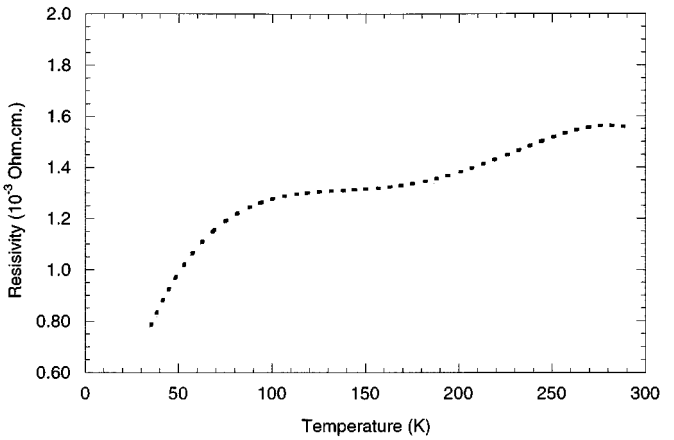

FIG. 10. Temperature variation of the electrical resistivity of $Sr_{0.07}La_{0.92}Mo_5O_8$.

The metallic and semiconducting properties observed in the series $Sr_{1-x}La_xMo_5O_8$ as function of x can be explained on the basis of a very simple band concept. Since there are two formula units of AMo_5O_8 per unit cell, there will be 32 and 34 electrons per Mo_{10} unit for $SrMo_5O_8$ and $LaMo_5O_8$ respectively, or 16 and 17 filled, two electron bands, which is consistent with the semiconducting behavior of these compounds. Starting with $LaMo_5O_8$, one can view the addition of Sr as removing electrons from the valence band of this phase, which at very low levels can be viewed as p-type doping, but at higher levels will result in metallic conductivity due to a partially filled band. A similar explanation of La substitution into $SrMo_5O_8$ will lead to n-type behavior and metallic conductivity. Qualitative Seebeck coefficient measurements show *n*-type behavior in both the Sr- and La-substituted end members, which confirms that electrons are the primary charge carriers. While this simple model serves to explain the behavior where significant amounts of both La and Sr are present, a more detailed examination of the band structure will be required to explain the anomalous low-temperature behavior of both the pure La compound and the lightly doped end members of this solid solution series.

Summary and Conclusions

The formation of a continuous solid solution between the isomorphous compounds $LaMo_5O_8$ and $SrMo_5O_8$ has been established. Although both end members are semiconductors, the solid solutions are metallic, at least when significant quantities of both La and Sr are present. This behavior can be interpreted in terms of a simple band model in which the replacement of La by Sr in $LaMo_5O_8$ removes

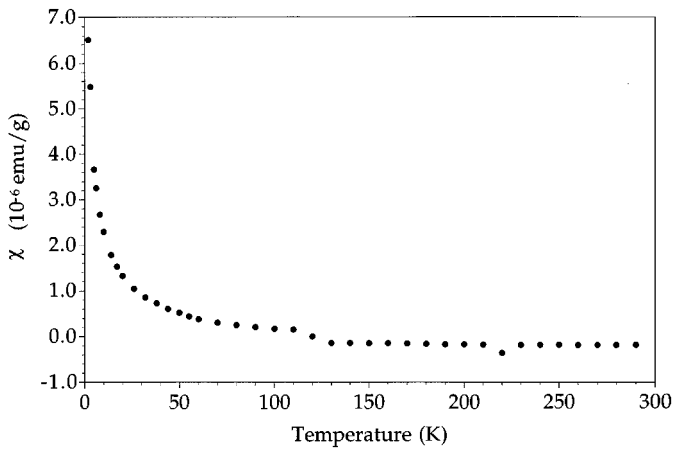

FIG. 9. Temperature variation of the magnetic susceptibility of $SrMo_5O_8$.

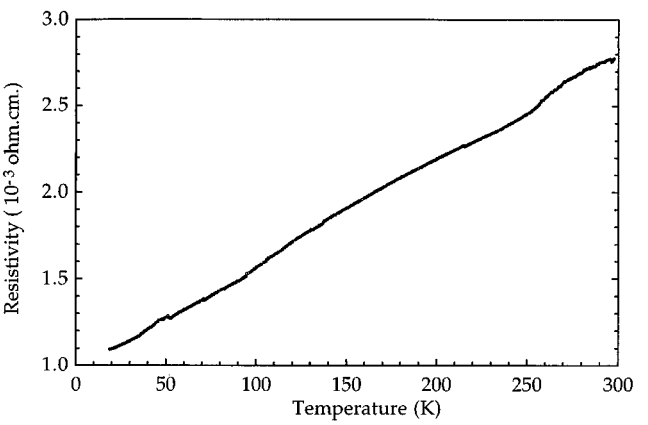

FIG. 11. Temperature variation of the electrical resistivity of $Sr_{0.52}La_{0.48}Mo_5O_8$.

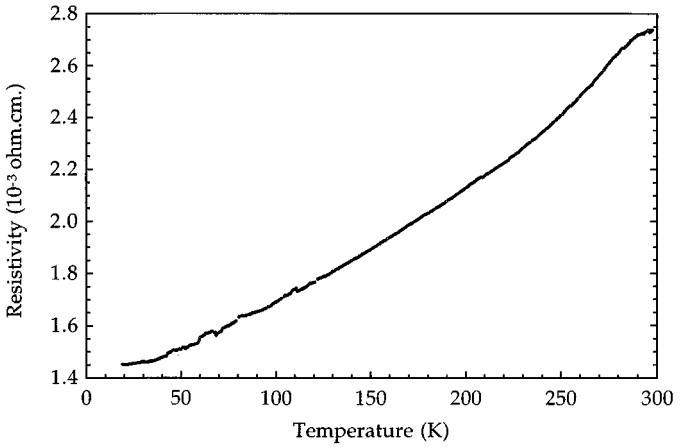

FIG. 12. Temperature variation of the electrical resistivity of $Sr_{0.83}La_{0.16}Mo_5O_8$.

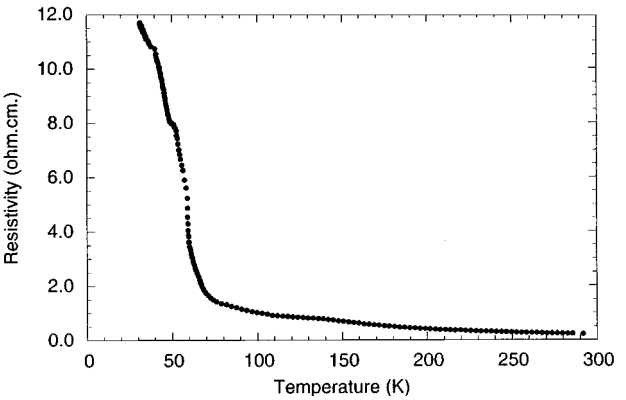

FIG. 14. Temperature variation of the electrical resistivity of $Sr_{0.955}La_{0.026}Mo_5O_8$.

electrons from the valence band and the replacement of Sr by La in $SrMo_5O_8$ adds electrons to the conduction band, ultimately resulting in a transition to metallic behavior. Dramatic changes in the electrical resistivities whose origins are yet to be explained were evident even at low levels of doping. A plausible explanation might be that both end members are on the verge of electronic instabilities, and subtle changes in the MCEs manifest themselves as drastic variations in the electronic properties. Single crystal X-ray diffraction studies of the solid solution members show no significant structural changes which can be correlated with the change from semiconducting to metallic behavior. Similarly, low-temperature neutron diffraction studies of pure $LaMo_5O_8$ gave no evidence that structural changes are associated with the low-temperature resistivity behavior observed for this compound.

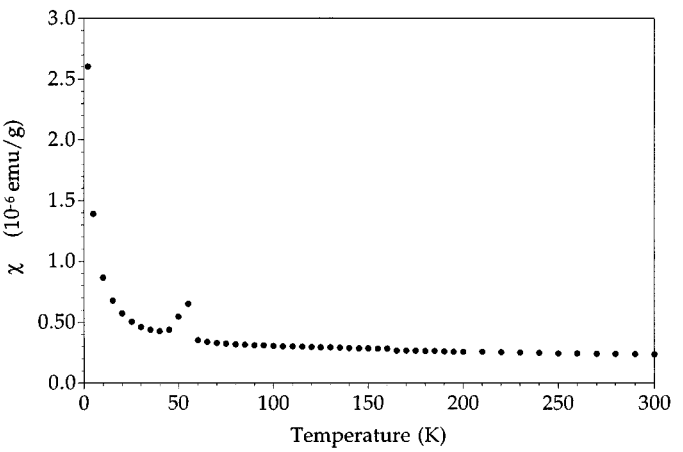

FIG. 13. Temperature variation of the magnetic susceptibility of $Sr_{0.52}La_{0.48}Mo_5O_8$.

ACKNOWLEDGMENTS

The work of W.H.M, M.B., K.V.R., and M.G. was supported in part by the National Science Foundation-Solid State Chemistry Grants, DMR-93-14605 and DMR-96-13106. K.V.R also acknowledges the release time awarded by Rowan University under a separately budgeted research grant. J.E.G. acknowledges the Natural Sciences and Engineering Research Council of Canada for a research grant and for support of DUALSPEC through a Major Facilities Access Grant.

REFERENCES

1. C. C. Torardi and R. E. McCarley, *J. Am. Chem. Soc.* **101,** 3963 (1979).
2. W. H. McCarroll, K. V. Ramanujachary, M. Greenblatt, and R. E. Marsh, *J. Solid State Chem.* **117,** 217 (1995).
3. C. C. Torardi, Ph.D. Thesis, Iowa State University, Ames, Iowa, 1981.
4. C. C. Torardi and R. E. McCarley, *J. Solid State Chem.* **37,** 393 (1981).
5. C. C. Torardi and R. E. McCarley, *J. Less-Common Met.* **116,** 169 (1986).
6. P. Gall, P. Gougeon, and R. E. McCarley, *Acta. Crystallogr. Sect. C* **44,** 1585 (1991).
7. R. E. McCarley, *Am. Chem. Soc. Symp. Ser.* **211,** 273 (1983).
8. R. E. McCarley, *Polyhedron* **5,** 51 (1986).
9. S. J. Hibble, A. K. Cheetham, A. R. L. Bogle, H. R. Wakerley, and D. E. Cox, *J. Am. Chem. Soc.* **110,** 3295 (1988).
10. P. Gall and P. Gougeon, *Acta Crystallogr. Sect. C* **50,** 7 (1994).
11. P. Gall and P. Gougeon, *Acta Crystallogr. Sect. C* **50,** 1183 (1994).
12. R. Dronskowski and A. Simon, *Angew. Chem., Int. Ed. Engl.* **6,** 758 (1989); R. Dronskowski, A. Simon, and W. Mertin, *Z. Anorg. Allg. Chem.* **602,** 49 (1991).
13. P. Gall, Doctoral Thesis, Universite de Rennes, Rennes, France, 1993.
14. P. Gougeon, M. Potel, and M. Sergent, *Acta Crystallogr. Sect. C* **46,** 1188 (1990).
15. P. Gall, P. Gougeon, M. Greenblatt, E. B. Jones, W. H. McCarroll, and K. V. Ramanujachary, *Croat. Chem. Acta* **68,** 849 (1995).
16. P. Gall, H. Noel, and P. Gougeon, *Mater. Res. Bull.* **28,** 1225 (1993).
17. A. C. T. North, D. C. Phillips, and F. S. Mathews, *Acta Crystallogr. Sect. A* **24,** 351 (1968).

18. G. M. Sheldrick, SHELXL93, "Program for the Refinement of Crystal Structures." University of Göttingen, Germany, 1993.
19. Enraf-Nonius, CAD-4 Software, Version 5.0. Enraf-Nonius, Delft, The Netherlands, 1989.
20. K. Fair, MOLEN User's Manual, "An interactive intelligent system for crystal structure analysis." Enraf-Nonius, Delft, The Netherlands, 1989.
21. J. Rodriguez-Carvajal, "FULLPROF, A Program for Rietveld Refinement and Pattern Matching Analysis," p. 27. Abstracts of the Satellite Meeting on Powder Diffraction of the XVth Congress of the I. U. C., Toulouse, France, 1990.
22. Quantum Design Technical Advisory MPMS #8, Quantum Design, Inc., 1990.